Real-Time Coded Excitation Imaging Using a CMUT-based Side Looking Array for Intravascular Ultrasound

Zangabad, Reza Pakdaman; Bosch, Johan G.; Mastik, Frits; Beurskens, Robert H.S.H.; Henneken, Vincent A.; Weekamp, Johannes W.; van der Steen, Antonius F.W.; van Soest, Gijs

DOI
10.1109/TUFFC.2021.3054971

Publication date
2021

Document Version
Final published version

Published in
IEEE Transactions on Ultrasonics, Ferroelectrics, and Frequency Control

This article has been accepted for publication in a future issue of this journal, but has not been fully edited. Content may change prior to final publication. Citation information: DOI 10.1109/TUFFC.2021.3054971, IEEE Transactions on Ultrasonics, Ferroelectrics, and Frequency Control

Real-Time Coded Excitation Imaging Using a CMUT-based Side Looking Array for Intravascular Ultrasound

Reza Pakdaman Zangabad*, Johan G. Bosch*, Frits Mastik*, Robert H.S.H. Beurskens*, Vincent A. Henneken‡, Johannes W. Weekamp‡, Antonius F.W. van der Steen*†§ and Gijs van Soest*
*Biomedical Engineering, Department of Cardiology, Erasmus MC University Medical Center Rotterdam, Rotterdam, the Netherlands
†Department of Imaging Science and Physics, Delft University of Technology, Delft, the Netherlands
‡Royal Philips NV, Philips Research, Eindhoven, the Netherlands
§Shenzhen Institutes of Advanced Technology, Chinese Academy of Sciences, Shenzhen, China

***Abstract*—Intravascular ultrasound (IVUS) is a well-established diagnostic method that provides images of the vessel wall and atherosclerotic plaques. We investigate the potential for phased-array IVUS utilizing Coded Excitation (CE) for improving the penetration depth and image signal-to-noise ratio (SNR). It is realized on a new experimental broadband Capacitive Micromachined Ultrasound Transducer (CMUT) array, operated in collapse mode, with 96 elements placed at the circumference of a catheter tip with $1.2\,\mathrm{mm}$ diameter. We characterized the array performance for CE imaging and showed that the -6 dB device bandwidth at 30 V DC biasing is 25 MHz with 20 MHz center frequency, with a transmit sensitivity of 37 kPa/V at that frequency.**

We designed a linear frequency modulation code to improve penetration depth by compensating high-frequency attenuation while preserving resolution by a mismatched filter reconstruction. We imaged a wire phantom and a human coronary artery plaque. By assessing the image quality of the reconstructed wire phantom image, we achieved $60\ \mu\mathrm{m}$ and $70\ \mu\mathrm{m}$ axial resolution using the short pulse and coded signal, respectively and gained 8 dB in SNR for coded excitation. Our developed system shows 20 frames per second, pixel-based beam-formed, real-time IVUS images.

***Index Terms*—CMUT, IVUS, Coronary Heart Disease, Coded Excitation, Atherosclerotic plaque, Mismatched Filtering, Pixel-based beam-forming**

I. Introduction

DISEASES of the heart and circulatory system (cardiovascular disease or CVD) are the main causes of death in Europe, accounting for 1.8 million deaths and more than 11 million hospitalizations each year in the EU[1]. More than a third (36%) of all deaths are from CVD. With an ageing population, the prevalence of many cardiovascular diseases increases strongly. The resulting economic, as well as human costs are tremendous. Overall, CVD is estimated to cost the EU economy almost 210 billion euros a year, due to healthcare costs and lost productivity.

Atherosclerosis, which is a chronic disease and asymptomatic at early stages, is characterized by the thickening of the vessel wall due to the buildup of plaque in the arterial intima [2]. In the coronary circulation, it is treated commonly by percutaneous coronary intervention (PCI): catheter-based balloon dilation and implantation of a stent. Intravascular Ultrasound (IVUS) is an established technique that images the vessel wall and atherosclerotic plaque [3] using a catheter-mounted transducer. It may be used to guide PCI and has significant outcomes benefits, including a 50% reduction in CV death after PCI [4], [5].

Commercial devices - either mechanically rotating single element or electronically scanned in a phased array configuration - use high frequency (20MHz-60MHz) piezoelectric transducers at the tip of a coronary catheter in order to assess the morphological properties of plaques and implanted stents. After two decades of relatively slow progress, innovations in IVUS imaging technology are now being introduced into the clinical arena. Improved resolution, dynamic range and image contrast may be valuable for identifying plaque components like calcification, lipid-rich necrotic core, and measuring the thickness of thin fibrous cap. Such parameters can inform an IVUS-guided PCI strategy.

In ultrasound imaging, signal-to-noise ratio (SNR) is a crucial factor for image quality. The high attenuation of the ultrasonic signals in the tissue results in echoes from large depths buried in noise. This attenuation depends on the ultrasound frequency, and is a significant limiting factor at the high frequencies used for IVUS imaging. Moreover, the image resolution requirements stipulate the transmission of short pulses, eventuating in relatively low transmitted signal energy and thus poor SNR. Increasing the transmitted power is limited by the maximum biological exposure to acoustic intensity, and by the capability of electronics (instruments and transducer materials) to handle such a high voltages.

Sophisticated signal transmission schemes have been developed in radar and mobile telecommunication systems [6], which are currently utilized in ultrasound imaging. Transmission of modulated signals, and decoding the received signal with an appropriate filter, can improve the SNR without degrading imaging resolution [7]. Different kinds of coded signals have been applied in medical ultrasound, predominantly chirp, linear frequency modulation (LFM), or pseudo-chirp excitation [8], [9], [10], while binary codes [11], [12] were also investigated.

This article has been accepted for publication in a future issue of this journal, but has not been fully edited. Content may change prior to final publication. Citation information: DOI 10.1109/TUFFC.2021.3054971, IEEE Transactions on Ultrasonics, Ferroelectrics, and Frequency Control

Phase-based binary codes like Golay and Barker codes have limited utility in ultrasound imaging, as the abrupt change in the phase of the coded signals produces higher harmonics. Since any ultrasound transducer acts as a band-pass filter, frequencies above the upper limit of the transducer frequency response are poorly transmitted, leading to imperfect encoding. On the other hand, it has been shown that linear FM signals have the best and most robust features for ultrasound imaging [13]. It is demonstrated that echos from linear FM signals can be processed without any depth-dependent filter compensation to retain the quality of the decoded signals. Consequently, it makes the processing less complicated.

The signal modulation and pulse compression can be described by a single measure of a signal: the time-bandwidth product (TB). The improvement in SNR due to the use of coded signal is equal to the TB product of the transmitted signal [14]. In ultrasound imaging, the system bandwidth is determined by the ultrasound transducer; thus, increasing the duration of the transmitted signal is the only way to increase the TB product. However, longer codes increase the deaf time: the time during which the transducer and/or driving electronics are not in receiving mode, which is undesirable. Utilizing a dedicated receiving and transmitting elements could circumvent the deaf time problem at a cost of higher complex arrays which might not be a good approach for IVUS application.

Coded excitation has previously been used for IVUS imaging. Maresca et al. [15] used chirp signals to investigate the vasa vasorum. Qiu et al. [16] introduced a coded excitation based IVUS system whose operation frequency was higher than 50 MHz. They showed that utilizing the modulated signal within that frequency range will improve the SNR and thus penetration depth, and makes IVUS image quality comparable with costly optical imaging systems. However, the deaf time in his system was 2.5 μs or 4 mm. This needs to be improved in order to make the system pragmatically utilizable in clinical application.

To date, IVUS transducer technology is predominantly based on piezoelectric materials. The major limitation of piezoelectrics is the inherent trade-off between bandwidth and sensitivity, which eventually limits image quality, and as argued above, is of key importance for the implementation of coded excitation schemes. Capacitive Micromachined Ultrasound Transducer (CMUT) is a promising alternative to piezoelectric transducers [17]. Advantages of CMUT over piezoelectric technology are the relatively large bandwidth with comparable sensitivity [18], [19], the freedom of geometric design [20], being lead free, ease of large-scale production (in semiconductor planar processing) and miniaturization which will lower the end product cost [21], [22], [23]. CMUTs are made of thin membranes which are essentially parallel plate capacitors with a gap between the plates. The acoustic properties can be dynamically adjusted by changing the DC bias voltage [24], [25]. Depending on the applied DC voltage, a CMUT works in either conventional or collapse mode, with considerably different acoustic and received noise behavior [26], [27]. All these properties offer great benefits for catheter-based forward looking and Side Looking-IVUS (SL-IVUS) applications [28], [29], [30], [31].

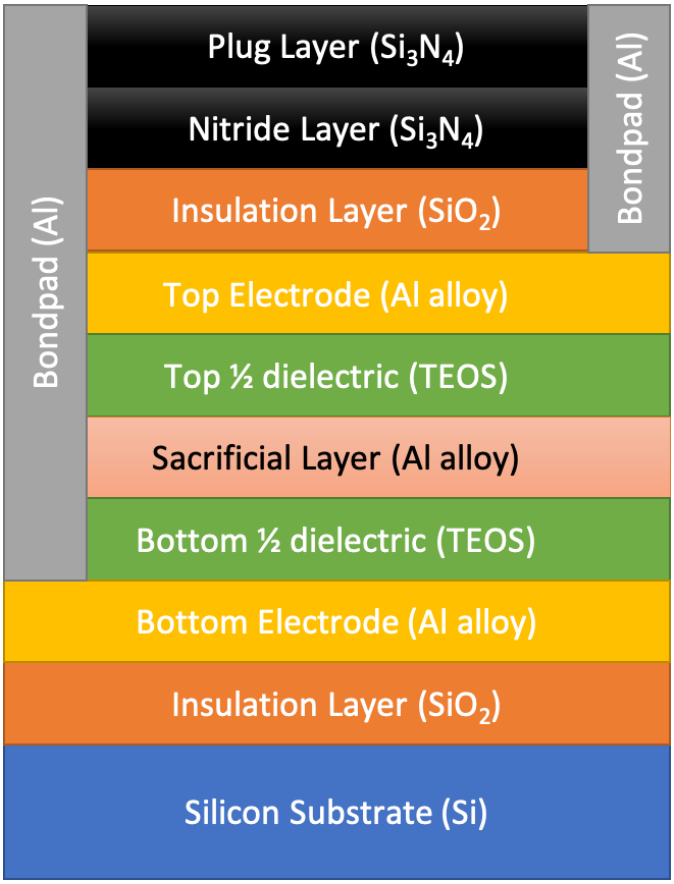

Fig. 1: Schematic view of the fabricated CMUT layers

In this work, we use a custom-designed CMUT IVUS sensor to investigate phased-array IVUS imaging using modulated signals. We operate the CMUT incollapse mode, to benefit from the enhanced bandwidth and sensitivity. According to the work published by Misaridis et al. [13], we chose appropriate coded waveforms and compression filters and designed a FM based coded signal suitable for IVUS imaging. The reconstructed signal and imaging characteristics are compared to a Gaussian pulse excitation, evaluated on a wire phantom target and on an *ex vivo* coronary artery specimen.

II. Materials and Methods

A. CMUT fabrication

The CMUT arrays were fabricated in a professional clean-room facility on a 6-inch silicon wafer utilizing the standard sacrificial release process, in which the cavity underneath the membrane is created by deposition and subsequent selective etching of a sacrificial metal layer [32]. Common processing steps were used to fabricate the transducer stack: metal sputtering, primer deposition, spinning of a photoresistive layer, patterning by means of light exposure over a photolithographic mask, photoresistive layer development, wet and dry etching, photoresistive layer stripping with acetone or oxygen plasma and plasma enhanced chemical vapor deposition of the insulating layer. The final transducer stack consists of a silicon wafer covered with silicon dioxide for passivation, a bottom electrode insulated with tetraethoxysilane (TEOS), vacuum

This article has been accepted for publication in a future issue of this journal, but has not been fully edited. Content may change prior to final publication. Citation information: DOI 10.1109/TUFFC.2021.3054971, IEEE Transactions on Ultrasonics, Ferroelectrics, and Frequency Control

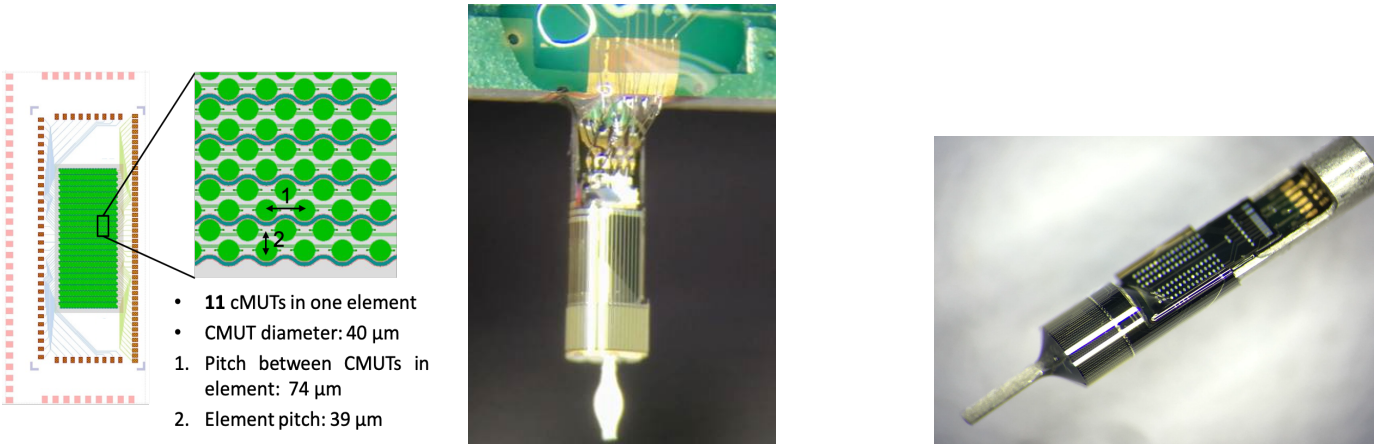

(a) (b) (c)

Fig. 2: **(a)** Layout of 48-element flat CMUT array and element geometry, **(b)** The rolled up 96-element CMUT array mounted on the PCB, as used for imaging, **(c)** The rolled-up array integrated in a catheter tip.

cavity created using the sacrificial release process, a TEOS insulated top metal electrode covered with silicon oxide and a nitride plug layer on the top. Apart from the plates, aluminum bond pads providing contact to the top or bottom electrodes are created on the side of the array to allow for wire bonding. More information on the patented fabrication of the CMUT can be found in [33], [24]. The complete layer stack including the layer materials is shown in Figure 1. The problem of charging in CMUTs are associated with charge carriers leaving from one electrode to the other. Based on this fabrication method, the isolation layers act as barriers for preventing or reducing the flow of charge carrier between the electrodes with the objective to fabricate charging-free CMUTs.

B. CMUT sensor design and assembly

A custom-designed CMUT array with 40 μm membrane diameter and 39 μm element pitch was manufactured by Philips Research. We characterized both a flat version of the 1-D CMUT array with 48 elements, and a 96-element array rolled up to catheter tip form factor. Figure 2a shows the schematic view of the linear CMUT array and the element geometry, consisting of 11 membranes. The same CMUT cells in a 96-element layout were wrapped around a catheter tip with 1.2 mm diameter, shown in Fig. 2c. The so-called Flex-to-Rigid (F2R) process allows the array to be rolled up into a cylinder shape. This enables the fabrication of arbitrary shaped silicon islands with co-integrated flexible connections including embedded flexible metal interconnects [34]. The cylindrical CMUT array was mounted on the side of a PCB for experiments.

The image sequence follows a sequential "transmit all, receive three" scheme, where the receive triplet is stepped across the array until all elements have been read out; acquisition of a full image requires 32 transmission/receive sequences. An application specific integrated circuit (ASIC) with low noise amplifier (LNA) was designed to address the elements in transmit and receive mode. In transmit mode, the ASIC allows the external AC signals to be applied to all transducer elements simultaneously. This design avoids the use of high-voltage ASIC technology and allows a more compact realization of the chip. In receive mode, the ASIC senses the echo signals of three selected transducer elements, and subsequently amplifies and buffers these signals to match the low impedance of the coax cables. The imaging fashion of excite all/receive three was stipulated by the ASIC. The LNA specifications are listed in Table I. The selection of the echo signals happens by means of a shift register that serves as a state machine.

The fabricated CMUT devices and the ASIC were glued and wire-bonded to the printed circuit board (PCB) and each other. The sample was coated with a thin layer of a silicone-like material for electrical insulation of the bond pads and passivation of the CMUT cells.

A custom made electronic unit, labelled "interface box" in Fig. 3 (Philips Innovation Services, Eindhoven, Netherlands), was used to pass the externally generated control signals to the ASIC. These controlled switching between transmit/receive mode and selected the next triplet of CMUT elements to receive the echo signal. The interface box also provided AC and DC amplification, externally controlled Time Gain Compensation (TGC) functionality, and protective circuitry to prevent high-voltage transmission to the ASIC while in receive mode. It provides 46 to 30 dB of RF amplification (8 MHz - 40 MHz) where the frequency response of the RF amplifier was compensated for in the excitation signals. The TGC has 12 to 81 dB amplification depending on its input level (0 V - 1.1 V) over the mentioned frequencies. The interface box provides

TABLE I: LNA Specifications

Specification	Value	Explanation
Signal bandwidth	30 MHz	AC transfer function, -3 dB roll off of receive chain
Gain	50 dB	LNA gain at 20 MHz with $Z_{\text{load}} = 75\,\Omega$
Noise Factor	4 dB	Noise factor at 20 MHz
Dynamic Range	75 dB	Over entire bandwidth
Channel Cross talk	-65 dB	Cross-talk of an unselected channel on the signal of a selected channel

This article has been accepted for publication in a future issue of this journal, but has not been fully edited. Content may change prior to final publication. Citation information: DOI 10.1109/TUFFC.2021.3054971, IEEE Transactions on Ultrasonics, Ferroelectrics, and Frequency Control

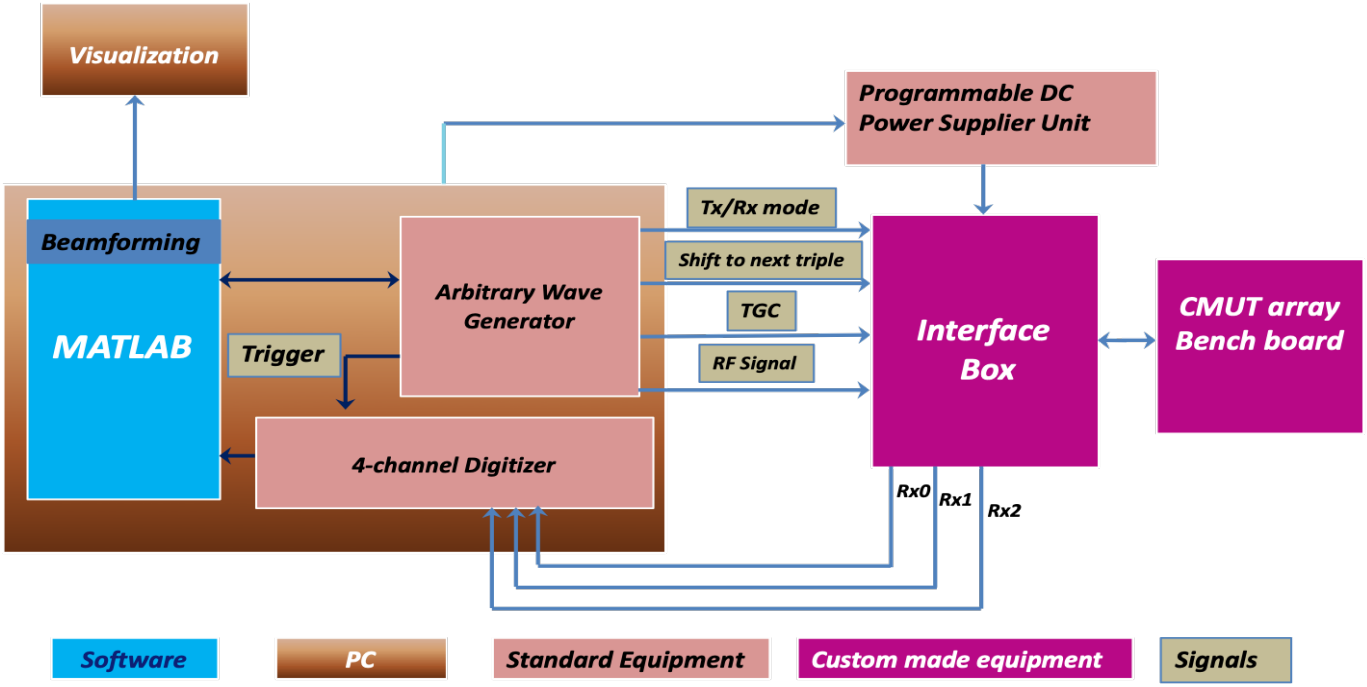

Fig. 3: IVUS system level description. Schematic block diagram of IVUS architecture, including main interactions.

45.9 dB DC amplification.

C. Characterization of the CMUT sample

The transmit impulse response of the CMUT array was measured in a water tank set-up. The PCB with the flat 48-element CMUT array was mounted on a three-axis manual translation stage, immersed in water and positioned at a distance of 3 mm from the tip of the calibrated 0.2 mm needle hydrophone (Precision Acoustics, Ltd, Dorset, UK). The CMUT array was biased at different voltages using a DC source (ADCMT; 6241A, ADC Corporation, Saitama, Japan) and was driven by a unipolar Gaussian pulse with an amplitude of 10 V and duration of 50 ns, generated by an arbitrary wave generator (DA4300, Chase Scientific Co., Langley, WA, USA), input to the custom RF amplifier. The voltage signal received on the hydrophone was digitized (Razor CSE1442; GaGe, Lockport, IL, USA). The block diagram of the system is shown in Fig. 3.

The CMUT array transmit response was measured as a function of bias voltage. Keeping the amplitude of the transmitted signal constant allowed for a uniform characterization of the transmit sensitivity. The bias voltage was increased from 0 V to 30 V with step of 2.5 V. The upper limit of 30 V was chosen so that the added bias and driving voltages would not exceed the maximum safe operating limit of 48 V on the CMUT. The CMUT array transitioned into collapse mode when a bias voltage of approximately 17.5 V was applied. The snap-back voltage was measured in a similar way, except with the order of the applied bias voltage being reversed. The array snap-back voltage was measured to be 15 V.

The voltage signal received on the hydrophone was converted into output pressure using the hydrophone calibration data (up to 40 MHz), and corrected for the RF amplifier frequency response, as well as the sound attenuation in water. Nonlinear propagation effects are neglected. The spectra of the received signals were analyzed and plotted as the frequency response of the CMUT array at different bias voltages. The center frequency, fractional bandwidth and transmit sensitivity were calculated as a function of the bias voltage. Using the full characterization of the flat array, we measured the output pressure of the rolled-up sensor using the hydrophone at optimal bias.

D. Coded Excitation

The basic principle of coded excitation and pulse compression is to convert a long frequency-modulated transmitted signal into a correlation signal with shorter time duration and a greater contrast to noise ratio. This happens by applying a matched filter, with an impulse response equal to the excitation waveform with reversed time axis. Therefore, if the input signal to the filter is the same as the excitation signal, the matched filter response would be mathematically equivalent to the auto-correlation of the transmitted signal. Any change, such as applying an apodization window to the matched filter impulse response, makes the filter "mismatched" with the input waveform.

In the presence of frequency dependent attenuation, LFM or chirp signals have the most robust performance in terms of SNR improvement [13]. The chirp signal of duration T may be formulated as:

$$s(t) = A\cos\left(2\pi\left(f_c.t + \frac{B}{2T}t^2\right) + \Phi_c\right) \ , \qquad (1)$$

where $0 < t < T$, f_c is the starting frequency, A is the signal amplitude, B is the chirp bandwidth and Φ_c is the starting phase. Based on the theory of the code compression, the expected gain in SNR is equal to the time-bandwidth product.

This article has been accepted for publication in a future issue of this journal, but has not been fully edited. Content may change prior to final publication. Citation information: DOI 10.1109/TUFFC.2021.3054971, IEEE Transactions on Ultrasonics, Ferroelectrics, and Frequency Control

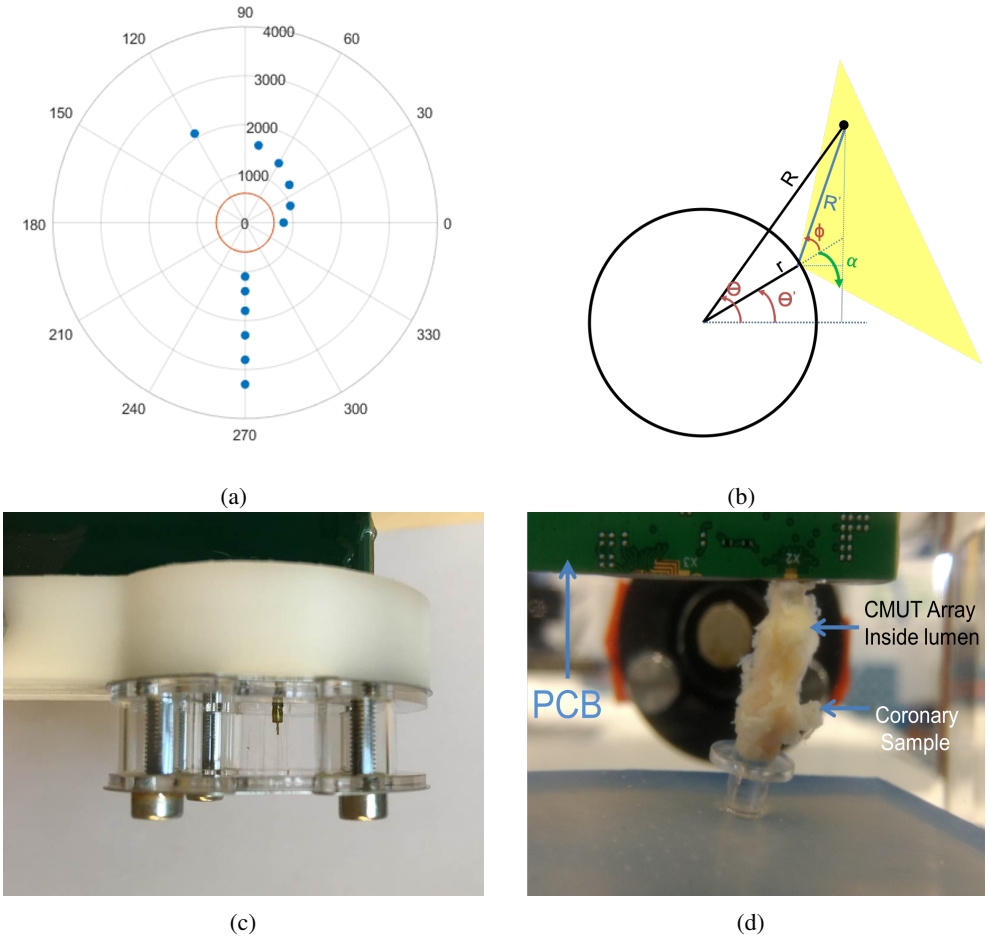

Fig. 4: **(a)** Schematic top view of the wire positions inside the phantom, **(b)** angular response from an individual array elements, **(c)** Rolled-up imaging core inside custom developed wire phantom. **(d)** Rolled-up imaging core inside an autopsy human coronary artery specimen

$$GSNR = T \times B \tag{2}$$

E. Wire phantom imaging

A wire phantom was designed to quantitatively evaluate the imaging resolution and depth of the rolled-up array. Figure 4a shows a top view of the wire positions inside the phantom. The tungsten wire diameter was 15 μm. The wire-phantom was mounted on the side of the PCB, such that the catheter tip is centered in the phantom. The complete assembly was immersed in water (Fig. 4c). We beam-formed all RF-lines acquired from the 96 elements in the GPU. Imaging performance was quantified in terms of the SNR and resolution, comparing images formed by a Gaussian short-pulse excitation and the compressed chirp.

F. IVUS Beamforming

In conventional dynamic focusing, the image is created line-by-line using a fixed transmit focus and a dynamic delay-and-sum receive focus which is then scan-converted to create virtual lines, to be interpolated in between the actual lines. In the approach we adopt here, a pixel based beam-forming scheme improves spatial resolution by lowering the interpolation artifacts. In this method, we assumed a virtual source behind the elements, at the center of the catheter, producing cylindrical waves. This is a useful assumption since all elements fire simultaneously.

For SL-IVUS imaging, a dense circular array of 96 elements was modeled for beam-forming. The elements were equally spaced around the circumference of the catheter at an element pitch of about half wavelength at the fundamental operation frequency of 20 MHz.

We examine the receive aperture per element based on the signal coming from a single fixed scatterer. Figure 4b depicts the parameters that affect the receive aperture. Knowing the angular response of the elements, we can attribute all the pixels within the region in which the echo signals are received (highlighted area) by each element.

$$R' = \sqrt{\left(R\cos(\theta) - r\cos(\theta')\right)^2 + \left(R\sin(\theta) - r\sin(\theta')\right)^2} \tag{3}$$

This article has been accepted for publication in a future issue of this journal, but has not been fully edited. Content may change prior to final publication. Citation information: DOI 10.1109/TUFFC.2021.3054971, IEEE Transactions on Ultrasonics, Ferroelectrics, and Frequency Control

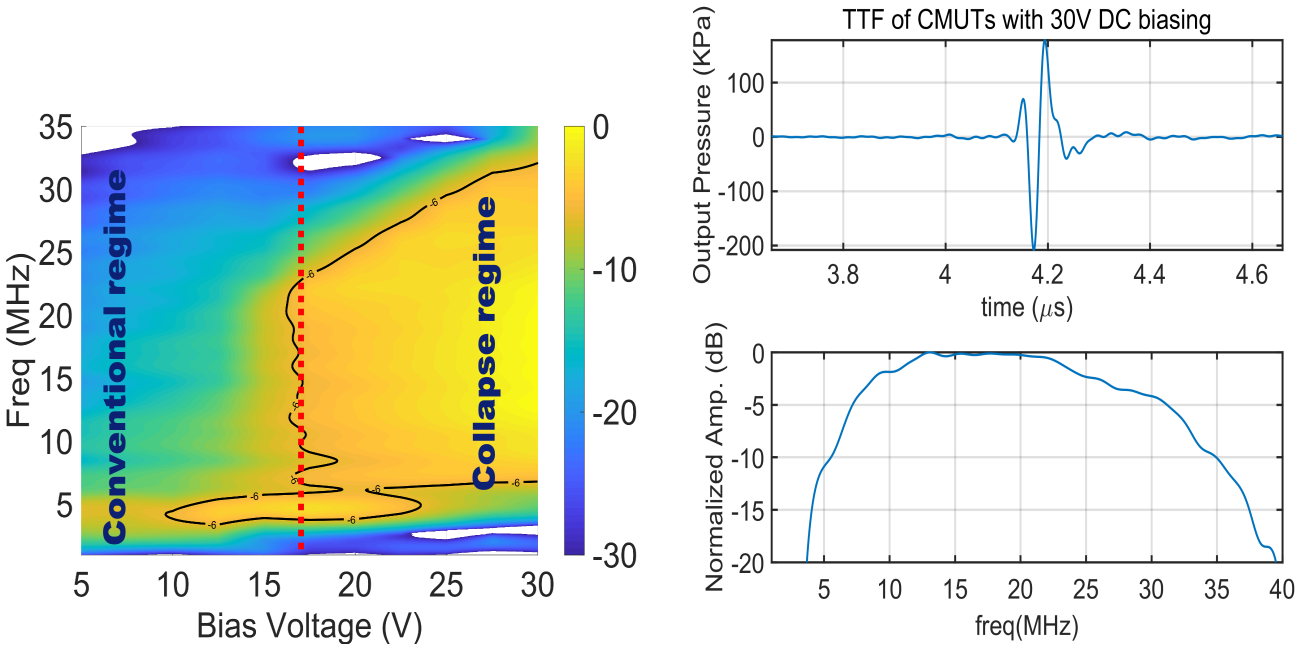

(a) (b)

Fig. 5: **(a)** Transmit Transfer Function of 48 elements CMUT array as a function of biasing voltage in dB relative to the maximum response, **(b)** Transmit transfer function and Sensitivity of CMUT array at 30 V DC biasing.

$$\varphi = \arctan\left[\frac{R\sin(\theta) - r\sin(\theta')}{R\cos(\theta) - r\cos(\theta')}\right] - \theta' \tag{4}$$

In (3), R is the radial position of the reconstructed pixel (scatterer), R' is the distance between the pixel and the element, r is the position of the element, θ is the angle of the pixel from the horizontal and θ' is the angular position of the element. φ in (4) is the angle with respect to the normal at an individual element.

Using these distances, we calculated the propagation delay from the virtual source in the center of the catheter, to the scattering position (i, j) and back to the receiving element. We furthermore defined a mask A which rejects pixels outside the opening angle $\alpha = 50^\circ$ (relative to the element normal), based on the reflection from a single wire in the unbeamformed channel data. The resulting image amplitude $S(i, j)$ was then computed by a straightforward delay-and-sum approach:

$$\begin{aligned} t_n(i,j) &= \frac{R(i,j) + R_n^{'}(i,j)}{c} \\ A_n(i,j) &= \begin{cases} 1; |\varphi_n(i,j)| \leqslant \alpha \\ 0; |\varphi_n(i,j)| > \alpha \end{cases} \\ S(i,j) &= \sum_{n=1}^{96} S_n\left(t_n(i,j)\right) \times A_n(i,j) \end{aligned} \tag{5}$$

In (5), $t_n(i, j)$ is the calculated propagation time from each pixel to the element *n*; S_n are the received element waveforms. In coded excitation imaging, S_n are the traces after filter compression. We implemented pixel-based beam-forming scheme with a grid spacing of $5\,\mu$m over a 2D space of $1\,\text{cm} \times 1\,\text{cm}$.

G. Autopsy tissue experiments

A coronary artery was harvested during autopsy at the Dept. of Pathology of the Erasmus MC, under a protocol sanctioned by the local ethics board. A short section of artery was mounted in the water tank and imaged using the rolled-up IVUS device. The coronary artery was immersed in Phosphate-buffered saline PBS(1X) for imaging (Fig. 4d). The diameter of the artery was approximately 2 mm.

After IVUS experiments, the tissue was fixed for 24 hours in formalin and subsequently processed. A series of 5 sections, each $5\mu m$ thick, were taken at locations every 250 μm to gain insight into the tissue appearance in the vicinity of the imaging plane. At each location, two sections were taken for routine hematoxylin/eosin (HE) and Oil Red O (ORO) staining.

III. Results

A. Characterization of the CMUT sample

Figure 5a shows the Transmit Transfer Function (TTF) of the 48-element CMUT array at varying bias voltage. The received signals are Fourier transformed to obtain the frequency response and normalized to the maximum value among all measurements. The maximum transmit sensitivity is observed at an applied bias voltage of 30 V, at which the CMUT resonates at center frequency of 19.5 MHz. The -6 dB contour plot in Fig. 5a illustrates that the array is wide-band after collapsing, which happens at 17.5 V DC biasing.

The center frequency, fractional bandwidth and transmit sensitivity are calculated at each bias voltage. Figure 5b shows that the array provides approximately 400 kPa output pressure when it is biased at 30 V DC. This translates to a transmit sensitivity of 36.8 kPa/V with 130% fractional bandwidth at

This article has been accepted for publication in a future issue of this journal, but has not been fully edited. Content may change prior to final publication. Citation information: DOI 10.1109/TUFFC.2021.3054971, IEEE Transactions on Ultrasonics, Ferroelectrics, and Frequency Control

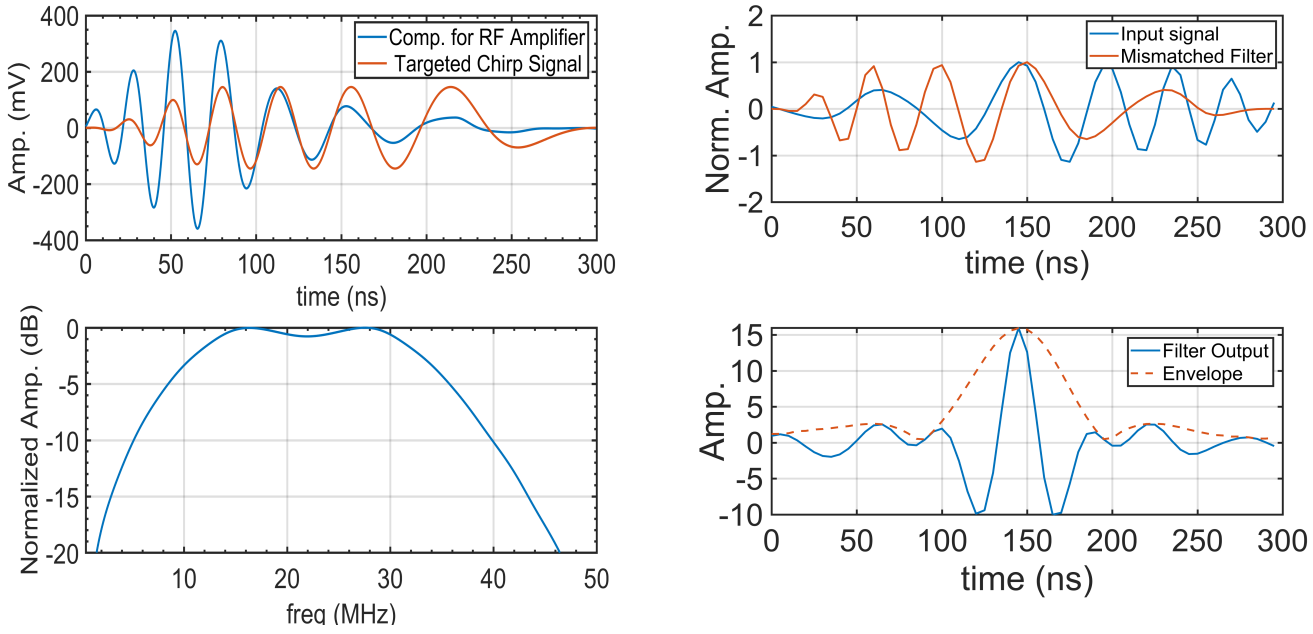

(a) (b)

Fig. 6: **(a)** Designed chirp signal and its compensation for the frequency dependant RF amplifier, **(b)** received signal and its mismatch filter response.

a center frequency of 19.5 MHz. For all subsequent imaging experiments, we adopted a bias voltage of 30 V.

Applying a bias voltage of 30 V, we quantified the transmitted pressure from the rolled-up array, which emits a cylindrical wave instead of a plane one. We found a transmit sensitivity of 7.8 kPa/V, recorded at the same delay of 4.2 μs.

B. Coded Excitation

Based on the characterization result of the CMUT sample, we designed a LFM signal with center frequency, $f_c = 22.4$ MHz, and 100% fractional bandwidth ($B = 22.4$ MHz). The LFM signal had a duration of $T = 300$ ns to meet the requirement of < 0.5 mm deaf-time for IVUS application. A Tukey tapered cosine window of 50% was applied to the LFM. The waveform amplitude was modulated to compensate for the frequency response of the RF amplifier (the blue line in Fig. 6a). The amplified chirp signal had the desired shape and frequency response, as depicted in Fig. 6a. Once the chirp is applied to the CMUT array, the impulse response of the CMUT again changes the waveform.

The received echo signal was considered as the input signal to the mismatched filter. Figure 6b illustrates the received signal from the wire and its complex conjugate, which was used as the mismatched filter response characteristic. The bottom part of Fig. 6b shows the output of the mismatched filter and its envelope. The width of the peak of the decoded signal envelope determines the resolution. The time-bandwidth product of the designed chirp signal was $T \times B = 6.7$ and based on the theory, we expect to gain 8.3 dB in SNR.

C. Imaging the wire phantom

The designed chirp signal was applied for imaging the wire phantom, compared to the short pulse for reference. Figures 7a and 7b correspond to the beamformed wire phantom image reconstruction of the Gaussian pulse and coded signal, respectively. The visual appearance of the pulsed and the coded images is similar. Quantitative evaluation of the image resolution was performed by making measurements in two perpendicular cross-sections through the reconstructed wire reflections, shown in Figs. 7c and 7d. The -6 dB axial and lateral resolutions of the short pulse and the coded excitation were found to be 60 μm, 70 μm and 270 μm, 245 μm, respectively, measured at a distance of 1.55 mm from the center of the catheter. Radial side lobes in the compressed chirp images were observed to be < 20 dB.

For the SNR calculation, we computed the ratio between the signal amplitude of a bright wire reflection (the red boxes in Figs. 7a and 7b) and the average amplitude in an area with only noise (blue boxes). We found an SNR of 32 dB for the short pulse image and 40 dB for the coded excitation image, confirming the 8 dB gain in SNR.

Pixel-based beamforming of the data was implemented in Matlab, achieving real-time acquisition and image formation at a maximum frame rate of 20 frames per second.

D. Ex-vivo imaging of the human coronary artery

We used the water tank set-up for real-time ex-vivo imaging the human coronary artery. We inserted the rolled-up array inside the lumen which was immersed in PBS. The designed chirp signal and the short pulse were used for imaging. Figure 8a shows a frame from the real-time IVUS images

This article has been accepted for publication in a future issue of this journal, but has not been fully edited. Content may change prior to final publication. Citation information: DOI 10.1109/TUFFC.2021.3054971, IEEE Transactions on Ultrasonics, Ferroelectrics, and Frequency Control

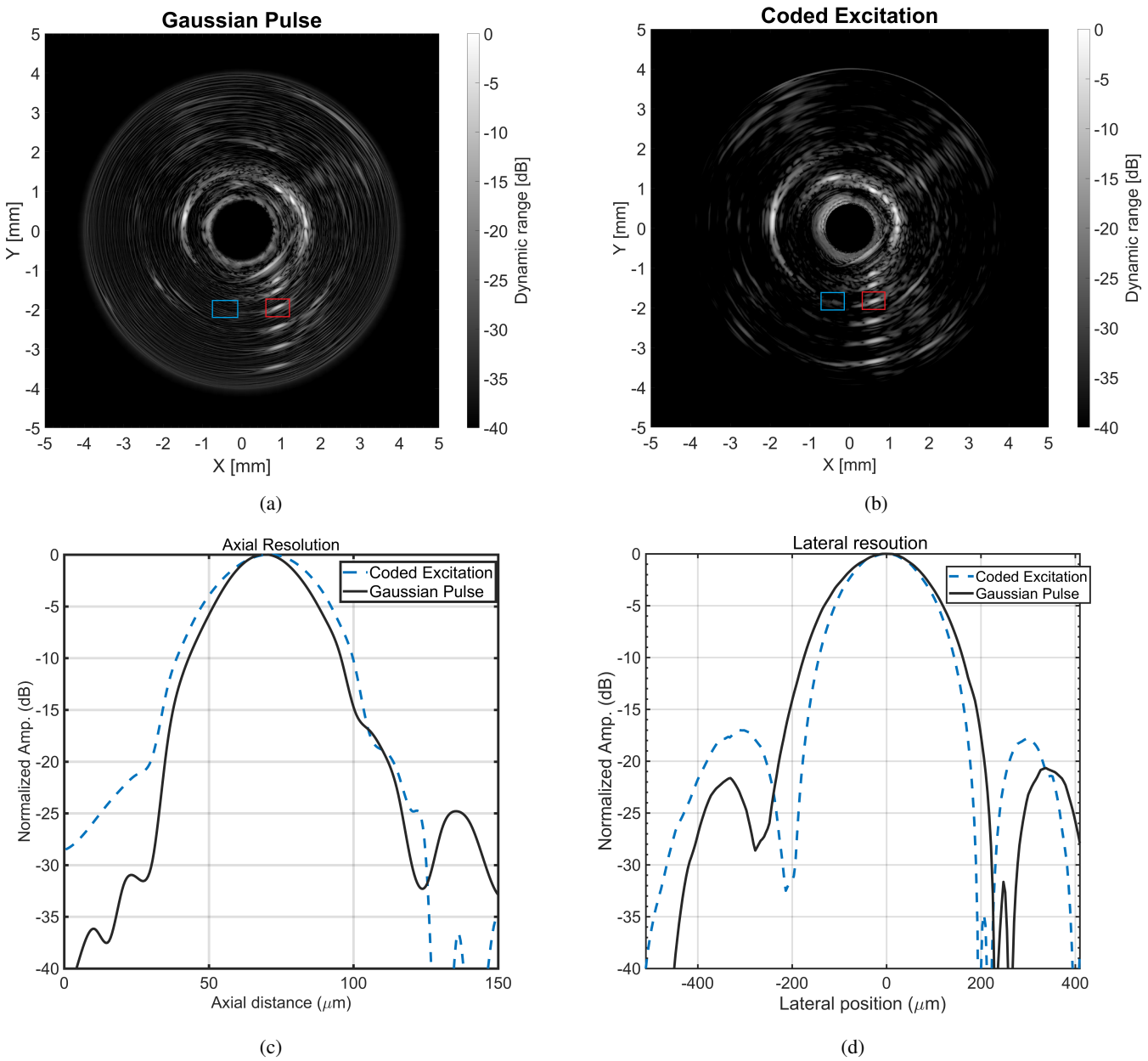

Fig. 7: Wire phantom image reconstruction using the short pulse **(a)** and the chirp signal **(b)** for the rolled-up CMUT array, **(c,d)** 60 μm axial resolution and 270 μm lateral resolution achieved using the short pulse (solid line) are compared with 70 μm axial and 245 μm lateral resolution achieved using the chirp signal.

obtained using the short pulse with dynamic range of 40 dB and Fig. 8b are corresponding to the IVUS images obtained by the chirp signal with dynamic range of 40 dB. Figure 8c shows the ORO histology image of the coronary sample where a big calcified region has been found, to which we attribute the bright reflection in the area at 1–5 o'clock in Figs. 8a and 8b.

IV. Discussion and Conclusion

This work focuses on the utilization of excitation codes for CMUT-based IVUS imaging. A state of the art CMUT array with 96 elements was fabricated and deployed for imaging.

We designed a linear frequency modulation (chirp) signal to improve signal to noise ratio while preserving resolution by a mismatched filter reconstruction. This method maximizes the combined use of the available bandwidth and transmission power. It can potentially improve the SNR and thus, the penetration depth of high-resolution IVUS. The device has a -6 dB device bandwidth at 30 V DC biasing of 25 MHz with 20 MHz center frequency and a transmit sensitivity of 37 kPa/V at that frequency.The chirp signal has 300 ns excitation time to meet the deaf-time requirement (less than 0.5 mm) for IVUS imaging. The transmitted acoustic power is limited by the voltage limits of the front-end electronics and the breakdown voltage of the CMUT.

We imaged a wire phantom and a human coronary artery. By assessing the image quality of the reconstructed wire phantom

This article has been accepted for publication in a future issue of this journal, but has not been fully edited. Content may change prior to final publication. Citation information: DOI 10.1109/TUFFC.2021.3054971, IEEE Transactions on Ultrasonics, Ferroelectrics, and Frequency Control

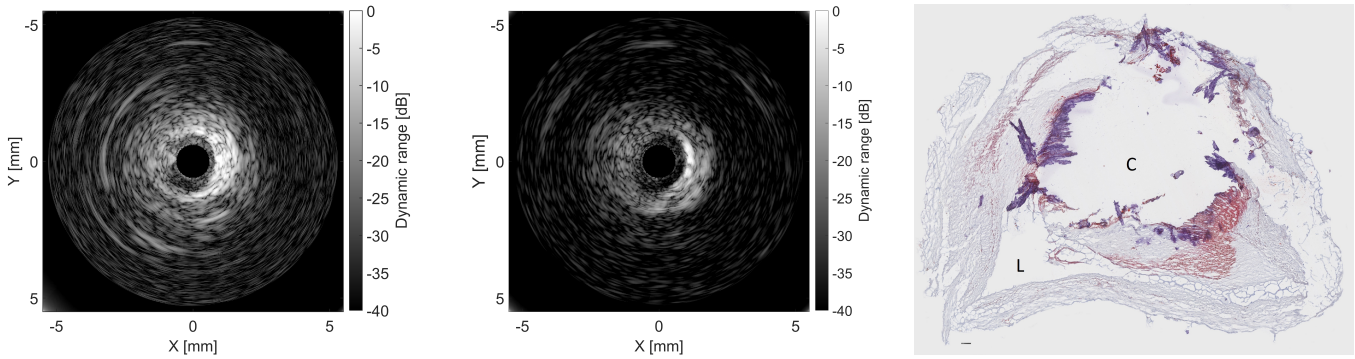

(a) (b) (c)

Fig. 8: Ex-vivo human coronary artery image reconstruction using the short pulse **(a)** and the chirp signal **(b)** by the rolled-up CMUT array. **(c)** is the histology image of the coronary sample. The scale bar is 100 μm

image, we achieve $60\mu m$ and $70\mu m$ axial resolution using the short pulse and coded signal, respectively. We showed that coded excitation improves SNR by 8 dB, at a cost of a slightly degraded axial resolution. This is due to the windowing/apodization which is used to lower the side-lobes associated with decoding the signal, reducing the effective bandwidth. However, it is sufficient for IVUS application. The imaging scheme that transmits on all elements and detects on consecutive triplets can potentially be improved. Selective excitation of transmission elements could improve the lateral resolution in the images, but this is currently not supported by the electronics.

We developed and demonstrated a system that provides 20 frame per second, real-time and pixel-based beamformed phased-array IVUS images and demonstrated the feasibility of intravascular ultrasound chirp imaging of human coronary atherosclerosis using the CMUT array. Features like a large calcification could be identified in both short-pulse and compressed-chirp imaging. Exact colocation of the imaged sections was challenging, which complicates a direct comparison of the two methods in imaging this very heterogeneous tissue.

We presented a novel concept for IVUS that exploits broad bandwidth offered by CMUT. We characterized the array performance for coded excitation imaging which may be useful for achieving greater penetration depth in IVUS while maintaining image resolution. CMUTs are manufactured using micromachining techniques which are evolved from the well-established integrated circuit fabrication process and possess unique potential in high yield mass production of CMUT-based IVUS catheters. Consequently, this technique offers an opportunity to lower the production costs. Future realizations may feature higher frequency, more compact and versatile transmit/receive electronics and dedicated image processing software for further improvements to image quality.

ACKNOWLEDGMENT

This work was done in the frame of the ENIAC INCITE project No. 621278. INCITE is an ENIAC JU project and is co-funded by grants from the Netherlands, Finland, Hungary, France, Ireland, Sweden, Spain, and Poland. The authors thank Dr. Deep Bera (Erasmus MC) for his support in beam-forming and Dr. Heleen van Beusekom and Matthijs Stam BSc (Erasmus MC) for preparing histology. We acknowledge assistance from Marcus Louwerse, Jeannet van Rens and Frank Budzelaar at Philips Research in realizing system components and devices under test, and valuable input from Martin Pekař at Philips Research in revising the manuscript.

REFERENCES

[1] E. Wilkins, L. Wilson, K. Wickramasinghe, P. Bhatnagar, J. Leal, R. Luengo-Fernandez, R. Burns, M. Rayner, and N. Townsend, *European Cardiovascular Disease Statistics 2017*. Belgium: European Heart Network, 2 2017.

[2] R. Ross, "The pathogenesis of atherosclerosis: a perspective for the 1990s," *Nature*, vol. 362, no. 6423, p. 801, 1993.

[3] A. Van Der Steen, R. A. Baldewsing, D. F. Levent, S. Emelianov, M. E. Frijlink, Y. Furukawa, D. Goertz, M. Karaman, P. T. Khuri-Yakub, K. Kim, *et al.*, "Ivus beyond the horizon." *EuroIntervention: journal of EuroPCR in collaboration with the Working Group on Interventional Cardiology of the European Society of Cardiology*, vol. 2, no. 1, p. 132, 2006.

[4] S.-J. Hong, B.-K. Kim, D.-H. Shin, C.-M. Nam, J.-S. Kim, Y.-G. Ko, D. Choi, T.-S. Kang, W.-C. Kang, A.-Y. Her, Y. H. Kim, S.-H. Hur, B.-K. Hong, H. Kwon, Y. Jang, M.-K. Hong, and for the IVUS-XPL Investigators, "Effect of Intravascular Ultrasound–Guided vs Angiography-Guided Everolimus-Eluting Stent Implantation: The IVUS-XPL Randomized Clinical TrialIntravascular Ultrasound–Guided Drug-Eluting Stent ImplantationIntravascular Ultrasound–Guided Drug-Eluting Stent Implantation," *JAMA*, vol. 314, no. 20, pp. 2155–2163, 11 2015.

[5] C. di Mario, K. C. Koskinas, and L. Räber, "Clinical benefit of ivus guidance for coronary stenting," *Journal of the American College of Cardiology*, vol. 72, no. 24, pp. 3138–3141, 2018.

[6] Y. Takeuchi, "An investigation of a spread energy method for medical ultrasound systems: Part one: Theory and investigation," *Ultrasonics*, vol. 17, no. 4, pp. 175–182, 1979.

[7] M. O'Donnell, "Coded excitation system for improving the penetration of real-time phased-array imaging systems," *IEEE transactions on ultrasonics, ferroelectrics, and frequency control*, vol. 39, no. 3, pp. 341–351, 1992.

[8] P.-C. Li, E. Ebbini, and M. O'Donnell, "A new filter design technique for coded excitation systems," *IEEE transactions on ultrasonics, ferroelectrics, and frequency control*, vol. 39, no. 6, pp. 693–699, 1992.

[9] M. Pollakowski and H. Ermert, "Chirp signal matching and signal power optimization in pulse-echo mode ultrasonic nondestructive testing," *IEEE transactions on ultrasonics, ferroelectrics, and frequency control*, vol. 41, no. 5, pp. 655–659, 1994.

[10] N. Rao, "Investigation of a pulse compression technique for medical ultrasound: A simulation study," *Medical and Biological Engineering and Computing*, vol. 32, no. 2, pp. 181–188, 1994.

[11] J. Shen and E. S. Ebbini, "A new coded-excitation ultrasound imaging system. i. basic principles," *IEEE transactions on ultrasonics, ferroelectrics, and frequency control*, vol. 43, no. 1, pp. 131–140, 1996.

[12] R. Kažys, L. Svilainis, and L. Mažeika, "Application of orthogonal ultrasonic signals and binaural processing for imaging of the environment," *Ultrasonics*, vol. 38, no. 1, pp. 171–175, 2000.

[13] T. Misaridis and J. A. Jensen, "Use of modulated excitation signals in medical ultrasound. part i: Basic concepts and expected benefits," *IEEE transactions on ultrasonics, ferroelectrics, and frequency control*, vol. 52, no. 2, pp. 177–191, 2005.

[14] T. Misaridis and J. A. Jensen, "Use of modulated excitation signals in medical ultrasound. part ii: design and performance for medical imaging applications," *IEEE Transactions on Ultrasonics, Ferroelectrics, and Frequency Control*, vol. 52, no. 2, pp. 192–207, Feb 2005.

[15] D. Maresca, K. Jansen, G. Renaud, G. van Soest, X. Li, Q. Zhou, N. de Jong, K. K. Shung, and A. Van der Steen, "Intravascular ultrasound chirp imaging," *Applied Physics Letters*, vol. 100, no. 4, p. 043703, 2012.

[16] W. Qiu, X. Wang, Y. Chen, Q. Fu, M. Su, L. Zhang, J. Xia, J. Dai, Y. Zhang, and H. Zheng, "Modulated excitation imaging system for intravascular ultrasound," *IEEE Transactions on Biomedical Engineering*, vol. 64, no. 8, pp. 1935–1942, 2017.

[17] B. T. Khuri-Yakub, F. Degertekin, X.-C. Jin, S. Calmes, I. Ladabaum, S. Hansen, and X. Zhang, "Silicon micromachined ultrasonic transducers," in *1998 IEEE Ultrasonics Symposium. Proceedings (Cat. No. 98CH36102)*, vol. 2. IEEE, 1998, pp. 985–991.

[18] O. Oralkan, B. Bayram, G. G. Yaralioglu, A. S. Ergun, M. Kupnik, D. T. Yeh, I. O. Wygant, and B. T. Khuri-Yakub, "Experimental characterization of collapse-mode cmut operation," *ieee transactions on ultrasonics, ferroelectrics, and frequency control*, vol. 53, no. 8, pp. 1513–1523, aug 2006.

[19] K. K. Park, O. Oralkan, and B. T. Khuri-Yakub, "A comparison between conventional and collapse-mode capacitive micromachined ultrasonic transducers in 10-mhz 1-d arrays," *IEEE transactions on ultrasonics, ferroelectrics, and frequency control*, vol. 60, no. 6, pp. 1245–1255, 2013.

[20] F. Y. Yamaner, S. Olcum, A. Bozkurt, H. Köymen, and A. Atalar, "Optimizing cmut geometry for high power," in *2010 IEEE International Ultrasonics Symposium*, IEEE. IEEE, oct 2010, pp. 2247–2250.

[21] D. T. Yeh, O. Oralkan, I. O. Wygant, M. O'Donnell, and B. T. Khuri-Yakub, "3-d ultrasound imaging using a forward-looking cmut ring array for intravascular/intracardiac applications," *IEEE transactions on ultrasonics, ferroelectrics, and frequency control*, vol. 53, no. 6, pp. 1202–1211, jun 2006.

[22] A. S. Savoia, G. Caliano, and M. Pappalardo, "A cmut probe for medical ultrasonography: From microfabrication to system integration," *IEEE transactions on ultrasonics, ferroelectrics, and frequency control*, vol. 59, no. 6, pp. 1127–1138, jun 2012.

[23] A. Caronti, G. Caliano, R. Carotenuto, A. Savoia, M. Pappalardo, E. Cianci, and V. Foglietti, "Capacitive micromachined ultrasonic transducer (cmut) arrays for medical imaging," *Microelectronics Journal*, vol. 37, no. 8, pp. 770–777, aug 2006.

[24] M. Pekař, W. U. Dittmer, N. Mihajlović, G. van Soest, and N. de Jong, "Frequency tuning of collapse-mode capacitive micromachined ultrasonic transducer," *Ultrasonics*, vol. 74, pp. 144–152, 2017.

[25] M. Pekař, A. F. Kolen, H. Belt, F. van Heesch, N. Mihajlović, I. E. Hoefer, T. Szili-Török, H. J. Vos, J. G. Bosch, G. van Soest, *et al.*, "Pre-clinical testing of frequency-tunable capacitive micromachined ultrasonic transducer probe prototypes," *Ultrasound in medicine & biology*, vol. 43, no. 9, pp. 2079–2085, 2017.

[26] S. Olcum, F. Y. Yamaner, A. Bozkurt, and A. Atalar, "Deep-collapse operation of capacitive micromachined ultrasonic transducers," *IEEE transactions on ultrasonics, ferroelectrics, and frequency control*, vol. 58, no. 11, pp. 2475–2483, nov 2011.

[27] R. P. Zangabad, A. Bozkurt, and G. Yaralioğlu, "Signal to noise ratio optimization for a cmut based medical ultrasound imaging system," in *2015 IEEE International Ultrasonics Symposium (IUS)*, IEEE. IEEE, oct 2015, pp. 1–4.

[28] F. L. Degertekin, R. O. Guldiken, and M. Karaman, "Annular-ring cmut arrays for forward-looking ivus: Transducer characterization and imaging," *IEEE transactions on ultrasonics, ferroelectrics, and frequency control*, vol. 53, no. 2, pp. 474–482, 2006.

[29] J. Zahorian, M. Hochman, T. Xu, S. Satir, G. Gurun, M. Karaman, and F. L. Degertekin, "Monolithic cmut-on-cmos integration for intravascular ultrasound applications," *IEEE transactions on ultrasonics, ferroelectrics, and frequency control*, vol. 58, no. 12, pp. 2659–2667, 2011.

[30] G. Gurun, C. Tekes, J. Zahorian, T. Xu, S. Satir, M. Karaman, J. Hasler, and F. L. Degertekin, "Single-chip cmut-on-cmos front-end system for real-time volumetric ivus and ice imaging," *IEEE transactions on ultrasonics, ferroelectrics, and frequency control*, vol. 61, no. 2, pp. 239–250, 2014.

[31] A. Şişman, J. Zahorian, G. Ö. Gürün, M. Karaman, M. Balantekin, F. L. Değertekin, and P. Hasler, "Evaluation of cmut annular arrays for side-looking ivus," in *2009 IEEE International Ultrasonics Symposium*. IEEE, 2009, pp. 988–991.

[32] A. S. Ergun, G. G. Yaralioglu, and B. T. Khuri-Yakub, "Capacitive micromachined ultrasonic transducers: Theory and technology," *Journal of aerospace engineering*, vol. 16, no. 2, pp. 76–84, 2003.

[33] J. H. Klootwijk, P. Dirksen, M. Mulder, and E. M. Moonen, "Capacitive micromachine ultrasound transducer," Sept. 15 2015, uS Patent 9,132,693.

[34] B. Mimoun, V. Henneken, A. van der Horst, and R. Dekker, "Flex-to-rigid (f2r): A generic platform for the fabrication and assembly of flexible sensors for minimally invasive instruments," *IEEE Sensors Journal*, vol. 13, no. 10, pp. 3873–3882, 2013.